Acta Crystallographica Section D
Biological Crystallography
ISSN 0907-4449

Conformational flexibility in the flap domains of ligand-free HIV protease

Holly Heaslet,[a]‡ Robin Rosenfeld,[b] Mike Giffin,[c] Ying-Chuan Lin,[a] Karen Tam,[a] Bruce E. Torbett,[c] John H. Elder,[a] Duncan E. McRee[b] and C. David Stout[a]*

[a]Department of Molecular Biology, The Scripps Research Institute, 10550 North Torrey Pines Road, La Jolla, CA 92037, USA, [b]Active Sight, 4045 Sorrento Valley Boulevard, San Diego, CA 92121, USA, and [c]Department of Molecular and Experimental Medicine, The Scripps Research Institute, 10550 North Torrey Pines Road, La Jolla, CA 92037, USA

‡ Current address: Pfizer Global Research and Development, Eastern Point Road, Groton, CT 06340, USA.

Correspondence e-mail: dave@scripps.edu

Received 11 April 2007
Accepted 13 June 2007

PDB References: HIV protease, wild-type, 1.4 Å, 2pc0, r2pc0sf; 2.15 Å, 2hb4, r2hb4sf; sixfold mutant, 2.3 Å, 2hb2, r2hb2sf.

The crystal structures of wild-type HIV protease (HIV PR) in the absence of substrate or inhibitor in two related crystal forms at 1.4 and 2.15 Å resolution are reported. In one crystal form HIV PR adopts an 'open' conformation with a 7.7 Å separation between the tips of the flaps in the homodimer. In the other crystal form the tips of the flaps are 'curled' towards the 80s loop, forming contacts across the local twofold axis. The 2.3 Å resolution crystal structure of a sixfold mutant of HIV PR in the absence of substrate or inhibitor is also reported. The mutant HIV PR, which evolved in response to treatment with the potent inhibitor TL-3, contains six point mutations relative to the wild-type enzyme (L24I, M46I, F53L, L63P, V77I, V82A). In this structure the flaps also adopt a 'curled' conformation, but are separated and not in contact. Comparison of the apo structures to those with TL-3 bound demonstrates the extent of conformational change induced by inhibitor binding, which includes reorganization of the packing between twofold-related flaps. Further comparison with six other apo HIV PR structures reveals that the 'open' and 'curled' conformations define two distinct families in HIV PR. These conformational states include hinge motion of residues at either end of the flaps, opening and closing the entire β-loop, and translational motion of the flap normal to the dimer twofold axis and relative to the 80s loop. The alternate conformations also entail changes in the β-turn at the tip of the flap. These observations provide insight into the plasticity of the flap domains, the nature of their motions and their critical role in binding substrates and inhibitors.

1. Introduction

HIV PR plays an essential role in HIV infection and replication by processing the Gag and Gag-Pol polyproteins produced during viral replication into the individual proteins required to form a mature virion (Elder *et al.*, 1993; Swanstrom & Wills, 1997; Pettit *et al.*, 1998; Lin *et al.*, 2006). HIV PR is a homodimeric aspartyl protease whose active site is formed across the twofold axis of symmetry relating the two polypeptides. The substrate-binding site runs lengthwise, perpendicular to the twofold, and is capped by flap domains formed by residues 45–54 from each subunit. These flap domains must open to allow access of substrate or inhibitors to the active site. HIV PR has been the target of drug development for more than a decade and protease inhibitors have drastically slowed the progression of disease and reduced the mortality

rate in HIV-1-infected patients (Swanstrom & Erona, 2000; Beck *et al.*, 2002; Kutilek *et al.*, 2003; Kozal, 2004). However, the development of multiple drug-resistant strains has regenerated interest in producing the next generation of protease inhibitors with broad-based specificity across many drug-resistant strains. In order to understand the mechanisms by which HIV PR evolves resistance while maintaining the ability to hydrolyze viral polyproteins efficiently and specifically, we have sought to observe alternate conformations of the flap domains and to characterize the structural changes induced by inhibitor binding.

The structural features of HIV-1 PR in the presence and absence of substrate or inhibitor have been compared in order to better understand the molecular basis of inhibitor binding and recognition. Conformational changes in the flaps upon binding peptides are known to be essential for specific recognition of Gag-Pol sequences (Prabu-Jeyabalan *et al.*, 2002, 2003). In the bound form of the enzyme, the packing of the flaps is also an essential aspect of substrate binding and drug resistance (Tozser *et al.*, 1997; Reiling *et al.*, 2002; Logsdon *et al.*, 2004; Prabu-Jeyabalan *et al.*, 2006). Mutation of residues in the flaps is associated with the evolution of drug resistance in clinical isolates (Kantor *et al.*, 2001) as well as in *in vitro* experiments (Shao *et al.*, 1997; Heaslet *et al.*, 2006). Flap mutations are second in importance only to changes in the substrate-binding site in conferring resistance to commercially available protease inhibitors. The presence of flap mutations (most commonly M46I) in conjunction with mutations in the substrate-binding cleft is commonly observed in isolates from patients treated with a single protease inhibitor but that are also cross-resistant to one or more additional drugs (Boden & Markowitz, 1998). Many of the flap residues observed in drug-resistant mutants are not involved in inhibitor interactions. Their ability to confer resistance is instead thought to be a result of effects on the ability of the flaps to open, allowing access to the substrate-binding site (Scott & Schiffer, 2000; Reiling *et al.*, 2002; Kurt *et al.*, 2003; Heaslet *et al.*, 2006). These aspects of the flap domains have been observed in previous studies of wild-type apo HIV PR in other crystal forms (PDB codes 2hvp, apo wild type, Navia *et al.*, 1989; 3hvp, apo wild type, Wlodawer *et al.*, 1989; 3phv, apo wild type, Lapatto *et al.*, 1989; 1hhp, apo wild type, BRU, Spinelli *et al.*, 1991) and in structures of apo forms of mutant HIV PR (PDB codes 1rpi, apo ninefold mutant, Logsdon *et al.*, 2004; 2g69, apo F53L, Liu *et al.*, 2006; 1tw7, apo tenfold mutant, Martin *et al.*, 2005). The capability of the flaps to undergo movements (Kurt *et al.*, 2003; Hou & Yu, 2007) is a critical component of the enzyme's ability to bind and cleave substrate (Scott & Schiffer, 2000; Tóth & Borics, 2006) and disruption of these movements could represent a novel mechanism for inhibiting the enzyme.

In our previous studies, wild-type HIV-NL4-3 was treated *ex vivo* with the broad-based inhibitor TL-3 in order to develop increasingly drug-resistant strains of the virus (Buhler *et al.*, 2001). These studies led to the formation of a TL-3-resistant strain encoding a protease in which six amino acids were mutated relative to the wild-type enzyme: 6× HIV PR (L24I, M46I, F53L, L63P, V77I, V82A). The sixfold mutations also resulted in an increased ability to cleave a peptide substrate relative to single (V82A) and threefold (M46I, F53L, V82A) mutants. The crystal structure of 6× HIV PR in complex with TL-3 revealed large conformational differences in the flap domains compared with the wild-type HIV PR–TL-3 complex (Heaslet *et al.*, 2006). These differences were ascribed to an increased ability to undergo induced-fit conformational change relative to the wild type and the single and threefold mutants.

In order to assess the intrinsic flexibility in the flaps and the nature of conformational change upon inhibitor binding, we have determined two new crystal structures of apo wild-type HIV PR and a structure of apo 6× HIV PR. These structures reveal two types of flap conformations in the absence of substrate or inhibitor: one in which the tips of the flaps 'curl' towards the 80s loop of the same subunit and away from the twofold-related monomer, and one in which they 'open' and shift away from the active site and each other. These two classes of flap conformations account for all apo HIV PR structures in the PDB (Berman *et al.*, 2000). Comparison of the apo HIV PR structures with those of complexes with TL-3 reveals distinct changes that occur upon transition from the 'open' or 'curled' conformations to a bound conformation. In this regard, the sixfold mutant displays a greater extent of induced fit. These results illustrate the structural plasticity of the flap regions with respect to the dynamics of flap opening and closure, and with respect to induced-fit recognition of substrates and inhibitors. Both phenomena represent mechanisms by which mutation can give rise to resistance.

2. Materials and methods

2.1. Cloning and expression

The cloning and expression of wild-type (NL4-3) and mutant (6×) HIV PR were performed as described previously (Lee *et al.*, 1998, 1999; Buhler *et al.*, 2001) and summarized below. A recombinant plasmid bearing a portion of the Pol gene of the BH10 clone of HIV was used for amplification of the sequence encoding the protease. The 5′ primer was constructed to insert an initiator methionine as part of the coding sequence for an *Nde*I site eight amino acids before the beginning of the protease. This primer also encoded a Q7K mutation to block a major site of autoproteolysis (Rose *et al.*, 1993). The 3′ primer was designed to insert a stop codon immediately after residue 99 of the protease and a *Hin*dIII site after the 3′ stop codon to facilitate directional cloning. The PCR product was then cut with *Nde*I and *Hin*dIII and inserted into the pET 21a+ vector (Novagen) for protein expression. Wild-type, single, threefold and sixfold mutant constructs (Heaslet *et al.*, 2006) were verified by DNA sequencing as previously reported (Buhler *et al.*, 2001). Recombinant plasmids were transformed into the BL21 (DE3) pLys S strain of *Escherichia coli* (Studier *et al.*, 1990). When the cells reached an OD_{600} of 0.8–1.0, expression was induced by adding 1 m*M* IPTG. The cells were then grown for between 4 h and over-

Table 1
Data-collection and refinement statistics.

Values in parentheses are for the highest resolution shell.

	Apo wild-type HIV PR	Apo wild-type HIV PR	Apo 6× HIV PR
PDB code	2pc0	2hb4	2hb2
Crystal data			
Space group	$P4_12_12$	$P4_12_12$	$P4_12_12$
Unit-cell parameters			
a (Å)	46.42	48.98	49.67
b (Å)	46.42	48.98	49.67
c (Å)	101.37	105.62	109.61
$\alpha = \beta = \gamma$ (°)	90	90	90
Solvent content (%)	50.1	57.0	59.7
V_M (Å^3 Da^{-1})	2.5	2.9	3.1
Molecules per ASU	1	1	1
Data collection			
Resolution (Å)	101.0–1.4	44.0–2.15	24.0–2.3
Unique reflections	27866	7074	6589
Observations	173096	99250	139873
R_{sym}† (%)	5.7 (52.2)	9.5 (60.1)	5.6 (37.6)
$I/\sigma(I)$	16.5 (3.0)	8.9 (2.2)	8.8 (2.0)
Completeness (%)	99.0 (98.0)	99.7 (99.5)	99.1 (99.7)
Mean multiplicity	6.2 (6.4)	7.3 (7.2)	9.1 (9.6)
Refinement			
Reflections used in refinement	21233	7074	6506
R_{cryst}‡ (%)	15.3	23.4	23.2
R_{free}‡ (%)	18.6	27.0	28.2
Reflections used in R_{free} ($\|F_o\| > 0$) (%)	5.2	5.3	4.7
R.m.s. deviations, bonds (Å)	0.008	0.023	0.010
R.m.s. deviations, angles (°)	1.20	2.10	1.24
Ramachandran plot (%)			
Favored	94.9	94.9	93.4
Allowed	5.1	5.1	6.6
Disallowed	0.0	0.0	0.0
Model			
Protein atoms (with alternate conformations)	842	789	777
Water molecules	111	40	21
Mg^{2+}	1	1	0
Average B factors (Å^2)			
Protein main-chain atoms	16.0	38.0	40.9
Protein side-chain atoms	18.3	38.5	41.0
Water molecules	30.8	41.7	38.0
Mg^{2+}	19.5	39.3	n/a

† $R_{sym} = \sum_{hkl}\sum_i |I_i(hkl) - \langle I(hkl)\rangle| / \sum_{hkl}\sum_i \langle I(hkl)\rangle$, where $I_i(hkl)$ is the intensity of an individual measurement and $\langle I(hkl)\rangle$ is the mean intensity of this reflection. ‡ R factors $= \sum_{hkl} |F_o| - |F_c| / \sum_{hkl} |F_o|$, where $|F_o|$ and $|F_c|$ are observed and calculated structure-factor amplitudes, respectively.

night at 310 K depending on which construct was being expressed.

2.2. Purification and refolding of mutant HIV PR

Inclusion bodies containing HIV PR were purified by resuspending the cell pellet from 1 l cell culture in 20 m*M* Tris–HCl, 2 mM EDTA pH 8.0 buffer containing 1% Np-40 and stirring for 20 min at RT. The solution was then treated in a Waring blender for 30 s. Inclusion bodies were pelleted at 8000*g* for 1 h and subsequently washed with deionized water until the pelleted inclusion bodies stuck to the side of the centrifuge tube (typically after the third wash). Inclusion bodies were solubilized in 8 *M* urea, 10 m*M* DTT with gentle rocking overnight at 277 K. Insoluble material was removed by centrifugation followed by filtration through a 0.45 µm membrane. Solid DE52 (Whatman; 20 g) was then added and the solution was incubated at 277 K for 1 h and filtered through a 0.45 µm membrane. The DE52 was discarded and the filtered solution containing the protease was applied onto an RQ column (J. T. Baker) that had been equilibrated in 8 *M* urea, 20 m*M* Tris–HCl, 2 m*M* EDTA pH 8.0. The column flowthrough containing the protease was collected and refolded by dialysis against 20 m*M* sodium phosphate pH 7.2, 25 m*M* NaCl, 10% glycerol and 0.2% 2-mercaptoethanol overnight at 277 K followed by dialysis against 10 m*M* sodium acetate pH 5.2, 0.2% 2-mercaptoethanol for 3 h. The refolded protease was centrifuged for 20 min at 38 000*g* and 277 K to remove any precipitated material. The sample was then concentrated using a centrifuge concentrator (Amicon Ultra, 10 000 molecular-weight cutoff), washed twice with 20 m*M* sodium acetate pH 5.2 and concentrated to 2–10 mg ml^{-1}.

2.3. Crystallization and data collection

2.3.1. Crystallization. Crystals of apo wild-type HIV PR were grown using two conditions. The 1.4 Å resolution structure was solved using crystals grown by mixing 1 µl HIV PR at 2.3 mg ml^{-1} with 1 µl of a solution consisting of 0.2 *M* $MgCl_2$, 20%(*w*/*v*) PEG 3350 and equilibrating by hanging-drop vapor diffusion at 277 K. Tetragonal bipyrimidal crystals formed within one week and were cryoprotected by quickly soaking the crystals in a solution containing the components of the crystallization reagent supplemented with 15% propylene glycol and flash-frozen in liquid N_2. The 2.15 Å resolution structure of apo wild-type HIV PR and the 2.3 Å resolution structure of apo 6× HIV PR were determined from crystals grown by mixing 1 µl HIV PR at 2.3 mg ml^{-1} with 1 µl of a solution consisting of 100 m*M* Tris–HCl pH 8.5, 0.2 *M* $MgCl_2$, 15%(*w*/*v*) PEG 8K and equilibrating by hanging-drop vapor diffusion at 277 K. Tetragonal bipyramidal crystals formed within one week and were cryoprotected in the mother liquor by addition of a solution containing 30% glycerol, incubation for 1–2 min, removal of a small amount of liquor and further addition of 30% glycerol. This process was repeated two more times and the crystals were harvested and flash-frozen in liquid N_2.

2.3.2. Data collection. Diffraction data for apo wild-type HIV PR were collected at 100 K using the rotation method (90 frames, 1° oscillation per frame) to 1.4 Å resolution at beamline 1-5 at the Stanford Synchrotron Radiation Labora-

tory (λ = 0.979 Å). The data were processed using *MOSFLM* (Leslie, 1992; Table 1). Diffraction data for apo wild-type and 6× HIV PR were collected at 100 K using the rotation method (120 frames, 1° oscillation per frame) to 2.15 and 2.3 Å resolution, respectively, on an Saturn 92 CCD system mounted on an FR-E X-ray generator equipped with VariMax optics (λ = 1.54 Å). The data were processed with *d*TREK* (Pflugrath, 1999; Table 1).

2.4. Structure solution and refinement

The structure of apo wild-type HIV PR in both crystal forms was solved by molecular replacement at 3.0 Å resolution using a monomer of the wild-type HIV PR–TL-3 complex structure (PDB 2az8) as a search model in *MOLREP* (Vagin & Teplyakov, 2000). A randomly selected 5% of reflections were designated as test reflections for use in the free *R* cross-validation method (Brünger, 1992) and were used throughout the refinement. The correlation coefficient and *R* factor from the molecular-replacement solutions indicated that the correct space group was $P4_12_12$. Rigid-body and restrained refinement were performed in *REFMAC* (Murshudov *et al.*, 1997) at 3.0 Å and then at 1.4 and 2.15 Å resolution for the two data sets. Simulated annealing, Powell minimization and individual temperature-factor refinement were performed using *CNS* (Brünger *et al.*, 1998). During the refinement of each wild-type HIV PR structure, the tips of the flaps were removed (residues 48–51) and the flap regions of the model were built into σ_A-weighted (Read, 1986) $|F_o| - |F_c|$ electron-density maps contoured at 2σ.

For the 1.4 Å resolution apo wild-type HIV PR data set, the model was further refined in *REFMAC* using anisotropic *B* factors with the addition of H atoms and the use of TLS refinement, followed by several rounds of model adjustment using σ_A-weighted $2|F_o| - |F_c|$ and $|F_o| - |F_c|$ electron-density maps generated in *Coot* (Emsley & Cowtan, 2004). 174 water molecules and one Mg^{2+} ion were added to the model and nine residues were modeled as having alternate side-chain conformations. The structure was refined to a final R_{cryst} and R_{free} of 15.3% and 18.6%, respectively (Table 1).

For the 2.15 Å resolution apo wild-type HIV PR data set, the model was refined in *CNS* using a bulk-solvent correction and isotropic *B* factors, followed by several rounds of model adjustment using σ_A-weighted $2|F_o| - |F_c|$ and $|F_o| - |F_c|$ electron-density maps. 168 water molecules and one Mg^{2+} ion were added and nine residues were modeled as having alternate side-chain conformations. The model was refined to a final R_{cryst} and R_{free} of 23.4% and 27.0%, respectively, in *CNS* (Table 1).

The structure of apo 6× HIV PR was solved by molecular replacement at 3.0 Å using a monomer of the 6× HIV PR–TL-3 complex structure (PDB code 2azc) as a search model in *MOLREP*. A randomly selected 5% of reflections were designated as test reflections for use in the free *R* cross-validation method and were used throughout the refinement. The correlation coefficient and *R* factor for the molecular-replacement solutions indicated that the correct space group was $P4_12_12$. Rigid-body and restrained refinement were performed in *REFMAC* at 3.0 and 2.0 Å, respectively. Simulated annealing, Powell minimization and individual temperature-factor refinements were performed using *CNS*. During the refinement, the tips of the flaps were removed and then rebuilt into positive regions of σ_A-weighted $|F_o| - |F_c|$ electron-density maps contoured at 2σ using the visualization program *O* (Jones *et al.*, 1991). The electron density for residues 48 and 49 and the side chain of residue 50 in the flaps was disordered and these residues could not be modeled. The model was refined using *CNS* with a bulk-solvent correction and isotropic *B* factors, followed by several rounds of model adjustment using σ_A-weighted $2|F_o| - |F_c|$ and $|F_o| - |F_c|$ electron-density maps. 21 water molecules were added and four residues were modeled as having alternate side-chain

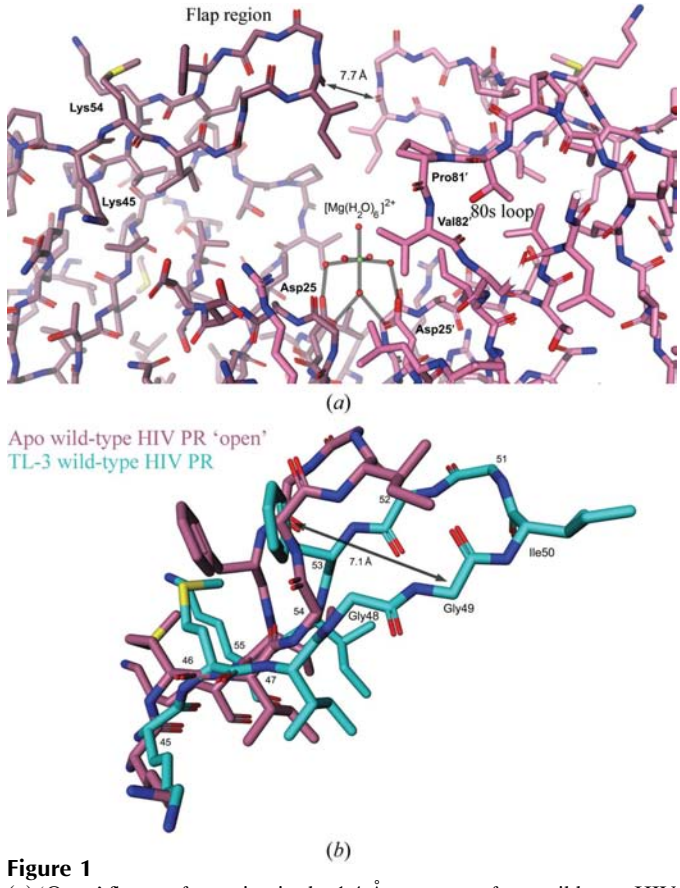

Figure 1
(*a*) 'Open' flap conformation in the 1.4 Å structure of apo wild-type HIV PR: view of the flaps, 80s loop and active site of unliganded wild-type HIV PR showing the 'open' configuration of the flaps. In the 'open' configuration the flaps are no closer than 7.7 Å apart and are not in contact with each other. The active site contains an $[Mg(H_2O)_6]^{2+}$ ion coordinated to the catalytic aspartates. (*b*) Comparison of the flap conformations of 'open' apo and TL-3-bound wild-type HIV PR. The conformation of the flap region (Lys45–Lys55) is significantly altered when comparing the unliganded form of the enzyme (rose) with the TL-3-bound form (cyan). In the TL-3-bound complex residues Gly48–Gly52 form a standard β-turn. In the 'open' conformation the turn is disrupted by large rotations about the φ, ψ torsion angles of Gly48 and Gly49, shifting it by 7.1 Å and orienting the Gly48-Gly49 peptide bond normal to the antiparallel β-strand of the flap. Consequently, the carbonyl O atom of Gly49 is flipped out of the plane of the flap and the β-turn hydrogen bond cannot be formed.

conformations. The model was refined to a final R_{cryst} and R_{free} of 23.2% and 28.2%, respectively, in *CNS* (Table 1).

2.5. TLS motion determination (TLSMD)

TLSMD analyzes a protein crystal structure for evidence of local or interdomain motion by partitioning the protein chains into multiple segments that are modeled as rigid bodies undergoing translation/libration/screw vibrational motion (Painter & Merritt, 2006*a*,*b*). The analysis generates all possible partitions up to a specified maximum number of TLS groups, in this case 17. Each trial partition is evaluated by how well it predicts the observed atomic displacement parameters (*B* factors) derived from crystallographic refinement. For the three structures evaluated, the fit between the predicted and observed displacement parameters was near-optimal when modeled as five segments.

3. Results

3.1. An apo form of wild-type HIV PR adopts an 'open' flap conformation

We determined two crystal structures of wild-type HIV PR in the absence of substrate or inhibitor. The first structure was determined to 1.4 Å resolution from crystals grown using 0.2 *M* $MgCl_2$ and 20% PEG 3350 as precipitant (Table 1). The crystals belong to space group $P4_12_12$ with a monomer in the asymmetric unit; the crystallographic twofold axis is coincident with the local twofold of the dimer. The TL-3 complex of wild-type HIV PR (PDB code 2az8) was used as the search model for molecular replacement. Difference Fourier maps indicated large conformational changes in the flap domains; subsequently, residues Lys45–Lys55 were removed from the model and rebuilt into unbiased $|F_o| - |F_c|$ maps contoured at 2σ. The refined structure shows that the tip of each flap is shifted ~4.5 Å away from the active site and the twofold axis. In this 'open' conformation, the flaps are separated by at least 7.7 Å and cannot form intermolecular hydrogen bonds or packing contacts (Fig. 1*a*).

The shift to an 'open' conformation occurs with a significant change in the main-chain geometry of residues Gly48–Gly52 at the tip of each flap. In the wild-type HIV PR–TL-3 complex these residues form a standard β-turn (Fig. 1*b*). In the 'open' conformation each strand is disrupted by large rotations about the φ, ψ torsion angles of Gly48, Gly49 and Ile54 (Fig. 1*b*), orienting the Gly48-Gly49 peptide bond normal to the antiparallel β-strands of the flap and flipping the carbonyl of Gly49 out of the plane of the flap. Consequently, the β-turn hydrogen bond cannot be formed and residues 45–55 of the loop are shifted away from the twofold-related flap.

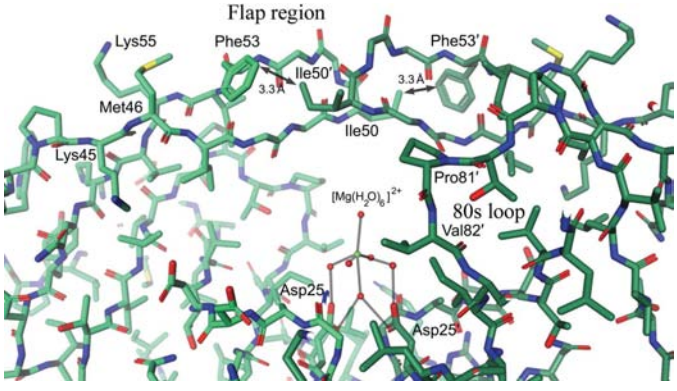

Figure 2
'Curled' flap conformation in the 2.15 Å structure of apo wild-type HIV PR: view of the flaps, 80s loop and active site of the unliganded wild-type HIV PR showing the 'curled' configuration of the flaps. In the 'curled' configuration the face of the antiparallel β-strand containing the side chains of Met46, Ile50 and Phe53 is adjacent to the same face of the flap in the twofold-related monomer (*i.e.* 'top-to-top'). In this conformation, the side chains of Phe53 and Ile50′ form a stabilizing packing contact. The active site contains an $[Mg(H_2O)_6]^{2+}$ ion coordinated to the catalytic aspartates, as in the 1.4 Å 'open' structure.

3.2. A second apo form of wild-type HIV PR adopts a 'curled' flap conformation

A second crystal form of apo wild-type HIV PR was grown using 0.2 *M* $MgCl_2$ and 15% PEG 8K as precipitant. These crystals exhibited expanded unit-cell parameters compared with the first form (Table 1). Examination of difference maps, relative to the wild-type HIV PR–TL-3 complex (PDB code 2az8) used as the molecular-replacement model, also indicated large conformational changes in the flap domains. To avoid averaging electron density at the ends of the flaps, the structure was initially refined in space group $P4_1$. Subsequently, the structure could be refined at 2.15 Å resolution in space group $P4_12_12$ with a monomer in the asymmetric unit and with the

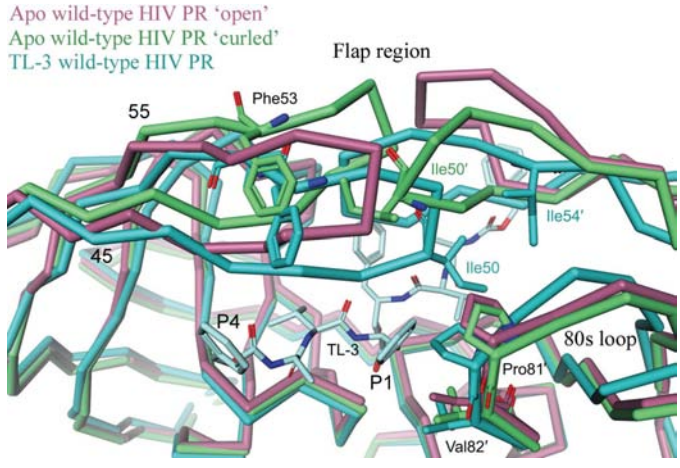

Figure 3
Flap conformational changes induced by binding of TL-3 to wild-type HIV PR. In the absence of substrate or inhibitor, the flap regions of wild-type HIV PR adopt two distinct conformations: 'open' (rose) and 'curled' (green). While the flap regions lack interactions in the 'open' conformation, a stabilizing packing interaction is formed between the side chains of Phe53 and Ile50′ of twofold-related monomers in the 'curled' conformation. Upon binding of TL-3 (cyan), the flaps shift toward the active site and their interactions are reconfigured: the side chain of Phe53 now interacts with the P4 benzyl group of TL-3 (light blue) and Ile50 contacts Ile54′. TL-3 also induces a shift in the 80s loop, which moves towards the inhibitor such that Pro81′ and Val82′ contact the P1 benzyl group.

crystallographic twofold coincident with the local twofold of the dimer (Table 1).

In the second apo wild-type HIV PR structure, the residues at the tips of the flaps, Gly48–Gly52, are shifted up to 6 Å toward the 80s loop (Thr80–Ile84) and away from the twofold-related monomer (Fig. 2). Surprisingly, the direction of movement is opposite to that seen in the 1.4 Å apo HIV PR structure (Fig. 3). As a result, the tips of the flaps adopt a 'curled' conformation in which residues 48–53 form interactions between monomers across the local twofold. This 'top-to-top' interaction of the flaps is characterized by symmetric contacts between surfaces displaying the side chains of residues Met46, Ile50 and Phe53 (Fig. 2). Distinct from the 'open' conformation, the tips of the flaps are packed together, allowing the side chain of Phe53 to interact with the side chain of Ile50′ from the other subunit. Despite their close proximity, the flaps do not form any intersubunit hydrogen bonds. The 'curled' conformation is also associated with contraction of the β-turn at the tip of the flap such that residues 49–52 adopt a 3_{10}-helical turn.

3.3. Both apo forms of wild-type HIV PR bind Mg^{2+} in the active site

While the active site of apo wild-type HIV PR is devoid of substrate or inhibitor, it does contain a coordinated $[Mg(H_2O)_6]^{2+}$ ion, as refined in both crystal forms (Table 1). The Mg^{2+} site presumably arises from the use of $MgCl_2$ in the crystallization conditions; it was modeled based on its electron density and octahedral coordination to six H_2O molecules at ∼2.1 Å distance. The $[Mg(H_2O)_6]^{2+}$ ion superposes on the twofold axis of the dimer such that three H_2O molecules form hydrogen bonds to all four O atoms of the catalytic aspartates Asp25 and Asp25′ (Figs. 1*a* and 2). One of these H_2O molecules, also on the twofold, corresponds to a H_2O molecule that hydrogen bonds to both Asp25 and Asp25′ in four TL-3 wild-type and inhibitor complexes (Heaslet *et al.*, 2006). The hydrated metal ion appears to provide electrostatic compensation and stabilizing interactions in the absence of bound substrate or inhibitor and may facilitate crystallization of the apo form, but it does not form any interactions with residues in the flap. The presence of $[Mg(H_2O)_6]^{2+}$ in both apo wild-type structures, in which the flap conformations differ significantly, implies that it does not influence the flap conformation.

3.4. The flap domains of apo 6× HIV PR also adopt a 'curled' conformation

Crystals of apo 6× HIV PR were grown using 0.2 *M* $MgCl_2$ and 15% PEG 8K as precipitant. Like the wild-type apo forms, the crystals belong to space group $P4_12_12$ with a monomer in the asymmetric unit, but in this case the unit cell is even larger (Table 1). Again, there was clear evidence from difference maps of conformational changes in the flap domains relative to the 6× HIV PR–TL3 complex used as the molecular-replacement model. Flap residues 45–55 of apo 6× HIV PR were removed from the model and rebuilt into difference electron density. The structure was refined in the higher symmetry space group $P4_12_12$ (Table 1).

Similar to the second form of wild-type HIV PR, the tips of the flaps adopt a 'curled' conformation. However, the disposition of the flaps is expanded so that they are ∼5 Å further apart and lack the intermolecular packing interactions seen in the 'curled' flap configuration of apo wild-type HIV PR (Fig. 4). At the same time, the side chain of Ile50 and residues Gly48 and Gly49 are disordered, which is indicative of greater flap flexibility in the sixfold mutant and consistent with observations for the TL-3 complex (Heaslet *et al.*, 2006). In the context of 6× HIV PR, the mutants M46I and F53L increase flap mobility owing to weaker packing interactions, resulting in both a decreased binding affinity for TL-3 and an increased activity relative to the single and threefold mutants. The 'curled' configuration in combination with greater separation allows the tip of the flap to shift even closer to the 80s loop, with the α-carbon of Ile50 within 4.1 Å of Pro81 (Fig. 4). This interaction, which is absent in the 'curled' form of apo wild-type HIV PR, presumably also involves the Ile50 side chain. The 'curled' conformation of apo wild-type HIV PR is characterized by intersubunit contacts involving Ile50 and Ile50′ with Phe53′ and Phe53, respectively (Fig. 2); in 6× HIV PR Phe53 is replaced by Leu, perhaps favoring the alternate interactions seen for Ile50 and Ile50′.

3.5. Flap conformations in the absence of substrate or inhibitor

Relative to the TL-3-bound form of HIV PR, two conformations of the flap domains have been captured in crystal forms of the apo wild-type enzyme: 'open' and 'curled'. The structures are expected to represent conformational states occurring during substrate binding and product release (Scott & Schiffer, 2000; Kurt *et al.*, 2003; Tóth & Borics, 2006). In the

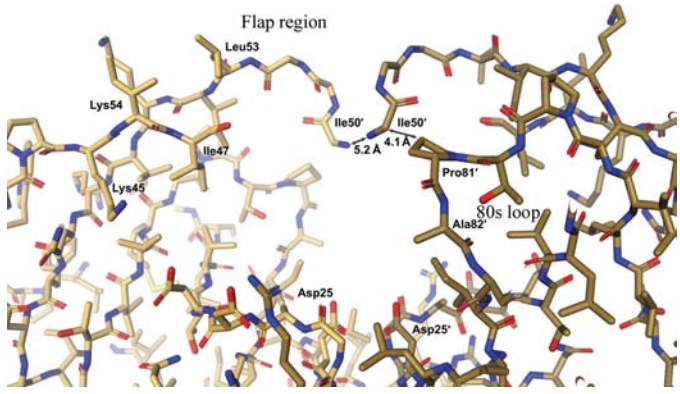

Figure 4
Expanded 'curled' flap conformation in the 2.3 Å structure of apo 6× HIV PR: view of the flaps, 80s loop and active site of the unliganded 6× HIV PR showing the expanded 'curled' configuration of the flaps. As in the 'curled' conformation of wild-type HIV PR, the flaps of 6× HIV PR adopt the 'top-to-top' orientation, but are ∼5 Å farther apart and lack stabilizing interactions. The flap residues Gly48 and Gly49 are disordered, along with the side chain of Ile50. The further expansion shifts the flaps toward the 80s loop, allowing a packing contact between Ile50 and Pro81 in the same subunit. The active site is devoid of ordered water molecules or metal ions.

'open' form the flaps are widely separated and exhibit a flattened β-turn at the tip of the loop (Fig. 1*b*). In the 'curled' conformation the flaps pack against each other *via* hydrophobic interactions in a 'top-to-top' configuration (Fig. 2). The flaps also shift significantly in opposite directions compared with the 'open' form, towards the 80s loop of the same subunit (Fig. 3). In the apo form of the sixfold mutant the flaps adopt a 'curled' conformation, but the structure is expanded such that the tips are no longer in direct contact (Fig. 4). Consequently, these conformations also entail translational displacements. Relative to the wild-type HIV PR–TL-3 structure and with the catalytic residue Asp25 as a reference point, Ile50 at the tip of the flap moves 2.1 Å away from, 3.7 Å toward and 6.8 Å toward Pro81 in the 80s loop in the 'open', 'curled' and expanded 'curled' forms, respectively.

3.6. TLS analysis of unliganded HIV PR

TLS thermal parameter analysis is a means of deriving correlated motions within protein structures by refinement against atomic *B* values (Painter & Merritt, 2006*a*,*b*). TLS parameters were derived for the unliganded crystal forms reported here to evaluate the translational and rotational motions of protein segments (see §2.5). For the structure of apo wild-type HIV PR in the 'open' conformation, flap residues 41–55 comprised a single TLS segment with 0.9 Å translational and 0.65 Å screw components for displacement roughly normal to the local twofold axis. Interestingly, this motion appears to be correlated with motion of the 80s loop (residue segment 80–99), such that the flap and 80s loop move in the same relative direction. For the structure with the 'curled' flap conformation, residues 44–54 define a TLS segment whose moment is almost perpendicular to the dimer twofold axis and which is also correlated with a TLS segment in the 80s loop. In this case, the amplitude of displacement is larger, with 1.5 Å translational and 1.0 Å screw components. Although residues 48 and 49 are disordered, flap residues 46–60 of apo 6× HIV PR form a TLS segment. The direction of displacement is similar to that in the apo wild-type structures, with 1.4 Å translational and 1.7 Å screw components. However, unlike the wild-type structures, this motion appears to be correlated with a segment in the catalytic loop (residues 25–38). Based on this analysis and consistent with the observed crystal structures, there are two principal components of conformational change in the flaps: (i) a hinge motion of residues 45 and 55, opening and closing the entire β-loop, and (ii) a translational motion of the flap normal to the dimer twofold toward or away from the 80s loop. The alternate conformations also entail changes in the β-turn at the tip of the flap (residues 49–52) and result in alternate packing interactions across the local twofold (Figs. 2 and 3).

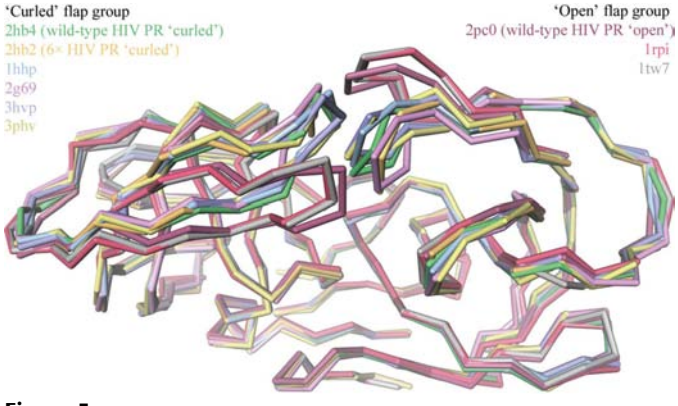

Figure 5
A comparison of nine structures of unliganded HIV PR. Superposition shows that there are two preferred conformations of the flaps in the absence of a ligand: 'curled' and 'open'. The majority of these structures (six of nine) fall into the 'curled' group, which entails 'top-to-top' interaction of the flaps. The comparison includes the three structures reported here, 2pc0 (1.4 Å wild-type HIV PR, rose), 2hb4 (2.15 Å wild-type HIV PR, green) and 2hb2 (2.3 Å 6× HIV PR, tan), and six previously reported structures, 3hvp (wild-type HIV PR, lavender; Wlodawer *et al.*, 1989), 3phv (wild-type HIV PR, yellow; Lapatto *et al.*, 1989), 1hhp (wild-type HIV PR, light blue; Spinelli *et al.*, 1991), 1rpi (9× HIV PR, magenta; Logsdon *et al.*, 2004), 2g69 (1× HIV PR, pink; Liu *et al.*, 2006) and 1tw7 (10× HIV PR, grey; Martin *et al.*, 2005). A seventh previously deposited structure, 2hvp (wild-type HIV PR; Navia *et al.*, 1989) comprises only C^{α} atoms.

4. Discussion

4.1. Conformational changes induced by TL-3 binding to wild-type HIV PR

The flexibility of the flaps is apparent upon comparison of the 'open' and 'curled' forms of apo HIV PR with the structure with TL-3 bound (Heaslet *et al.*, 2006). Inhibitor binding requires the flaps to close and undergo a significant reorganization (Fig. 3). This involves repacking the flap contacts from 'top-to-top' (Fig. 3, green) to 'bottom-to-bottom' (Fig. 3, cyan), accompanied by translational shifts with respect to the active site. In the 'top-to-top' interaction, as in the 'curled' form, the flaps exhibit contacts between the side chains of Phe53 and Ile50′ across the local twofold (Fig. 2). In the 'bottom-to-bottom' interaction, the tops of the flaps face away from each other, the side chains of Ile50 and Ile54′ are in contact and Phe53 interacts with the P4 phenyl ring of TL-3 (Fig. 3). TL-3 also induces multiple new contacts within the active site. For example, the P1 phenyl group inserts between the flap and the 80s loop, which shifts toward the inhibitor by ∼2 Å (Fig. 3). Relative to the apo wild-type structures, TL-3 binding precludes the presence of bound $[Mg(H_2O)_6]^{2+}$ and results in the displacement of ∼20 ordered water molecules.

4.2. Conformational changes induced by TL-3 binding to 6× HIV PR

Analysis of induced-fit changes in the flaps of 6× HIV PR is complicated by the fact that the TL-3 complex is asymmetric. One flap is farther from the active site and interacts with the inhibitor in a significantly altered conformation that entails flipping of the peptide bond between the P3 and P4 sites of the peptidomimetic inhibitor in one side of the active site (supplementary Fig. 1*a*[1]; Heaslet *et al.*, 2006). In contrast, on

[1] Supplementary material has been deposited in the IUCr electronic archive (Reference: YT5001). Services for accessing this material are described at the back of the journal.

the 'nonflipped' side of the active site the flap is 3 Å closer to the bound inhibitor and adopts a conformation similar to that seen in the TL-3 complex of wild-type HIV PR (supplementary Fig. 1*b*). However, this flap undergoes the largest shift upon TL-3 binding, moving 8.3 Å toward the active site; the flap on the 'flipped' side moves 6.3 Å. Conversely, the conformational change in the 80s loop is greater on the 'flipped' side where Pro81 forms tighter contacts with the P1 phenyl group (supplementary Figs. 1*a* and 1*b*). As in the wild type, the 'curled' flap conformation in 6× HIV PR undergoes a rearrangement from a 'top-to-top' configuration (although not in contact; Fig. 4) to a 'bottom-to-bottom' configuration upon binding TL-3.

4.3. Comparison of flap conformations in nine apo HIV PR crystal forms

Including the three structures reported here, nine available structures of apo HIV PR can be superposed (Fig. 5). All apo HIV PR variants crystallize in space groups $P4_1$ or $P4_12_12$. Although the flaps adopt different conformations with respect to the local twofold axis of the HIV PR dimer, the packing environments are similar. In other words, a common tetragonal lattice is observed in which the local twofold can coincide with a crystallographic twofold axis. Flaps that adopt the 'open' conformation have crystal-packing contacts with residues 39, 41 and 61 of twofold-related molecules in the lattice (supplementary Fig. 2*a*). Flaps that adopt the 'curled' conformation have contacts with the same two symmetry-related molecules, but in this case involving residues 61, 72 and 92 (supplementary Fig. 2*b*). While it is possible that the packing environment influences the flap conformation, there are nevertheless only two sets of lattice contacts observed.

Despite a range of mutational variants and crystallization conditions, the flap conformations observed in nine available structures fall into two groups (Fig. 5). The majority (six of nine) are 'curled' as in the 2.15 Å structure of apo wild-type HIV PR (Fig. 2), where the face of the antiparallel β-strand containing the side chains of Met46, Ile50 and Phe53 is adjacent to the same face on the twofold-related monomer (Fig. 6*a*). In this arrangement, intersubunit packing contacts are formed between the side chains of Phe53 and Ile50′, *i.e.* the 'top-to-top' configuration. The exceptions to this group are apo F53L HIV PR (PDB code 2g69; Liu *et al.*, 2006) and apo 6× HIV PR. In these structures the flaps are separated, *i.e.* expanded, and are not in contact (Fig. 4). Because 6× HIV PR contains the same flap mutation, Phe53Leu, it appears that Phe53 is required to stabilize the 'top-to-top' packing interaction *via* interaction with both Met46 and Ile50′ (Fig. 6*a*).

The other three apo structures include the 1.4 Å structure of wild-type HIV PR reported here and the structures of two multisite mutants, PDB codes 1rpi (9×) and 1tw7 (10×) (Figs. 5 and 6*b*). In these structures the flaps adopt the 'open' conformation, ∼10 Å apart, and no longer interact with one another (Fig. 3). In the 9× and 10× mutants the Met46Leu and Ile54Val mutations could be expected to affect the hinge. Our observation of an 'open' form of apo wild-type HIV PR demonstrates that this conformation is not dependent on the presence of resistance-inducing mutations. In general, the interactions of residues 46, 50, 53, 54 and 79 are relevant to interpreting the effects of mutations on the flaps (Figs. 6*a* and 6*b*). In the 'curled' group, the residues at positions 46 and 54 are Met and Ile, with one exception. In the 'open' group, the residues at positions 46 and 54 are Leu and Val, except for wild-type HIV PR, which can adopt both conformations (Fig. 5). In the 'curled' group Ile54 in the flap interacts with Pro79 in the 80s loop, but in the 'open' group the residues at these positions do not interact. It is apparent that relatively subtle mutations of hydrophobic residues at positions 46, 50, 53, 54 and 79 can stabilize either the 'curled' or 'open' conformations of the flaps.

4.4. Conformational transitions and inhibitor design

Molecular-dynamics simulations have modeled the 'open' conformation of the flaps required to allow substrate access to

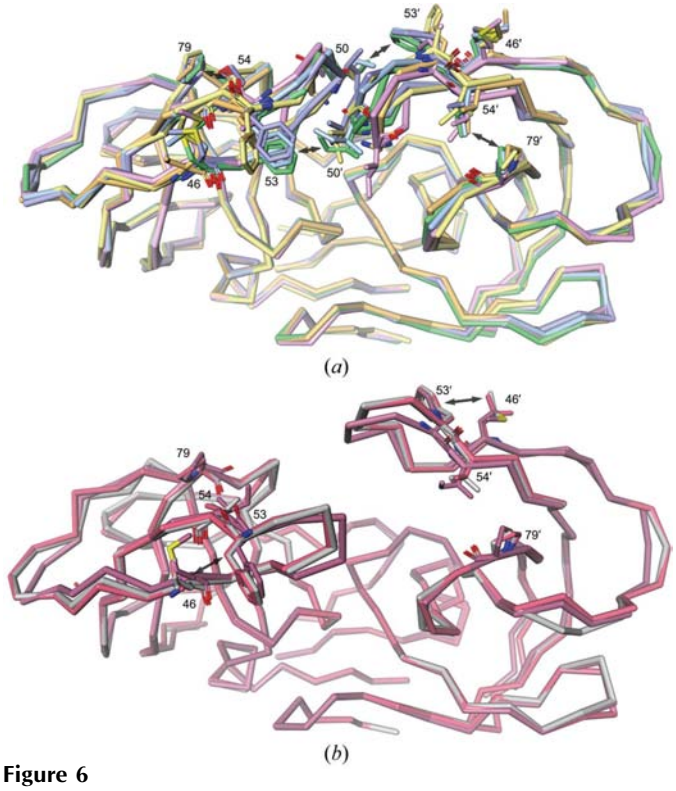

Figure 6
(*a*) The 'curled'-flap group of unliganded HIV PR structures. This group includes the two of the structures reported here, 2hb4 (2.15 Å wild-type HIV PR, green) and 2hb2 (2.3 Å 6× HIV PR, tan), and four others previously reported, 3hvp (wild-type HIV PR, lavender; Wlodawer *et al.*, 1989), 3phv (wild-type HIV PR, yellow; Lapatto *et al.*, 1989), 1hhp (wild-type HIV PR, light blue; Spinelli *et al.*, 1991), 2g69 (1× HIV PR, pink; Liu *et al.*, 2006). The 'curled' group is characterized by inter-flap interactions between residues 53 and 50′ and intra-subunit interactions between residues 46 and 53 and residues 54 and 79. (*b*) The 'open'-flap group of unliganded HIV PR structures. This group includes one of the structures reported here, 2pc0 (1.4 Å wild-type HIV PR, rose), and two others previously reported, 1rpi (9× HIV PR, magenta; Logsdon *et al.*, 2004) and 1tw7 (10× HIV PR, grey; Martin *et al.*, 2005). The 'open' group is characterized by intra-flap interactions between the side chains of residues 46 and 53, not 54 and 79, and a lack of inter-flap interactions.

the active site (Scott & Schiffer, 2000; Kurt *et al.*, 2003; Tóth & Borics, 2006). Starting from the 'curled' conformation observed in crystal structures of unliganded HIV PR (*i.e.* Fig. 5), the calculations reveal that the flaps can adopt an ensemble of conformations ranging from 'curled' to fully 'open'. During the transition the tips of the flaps become separated so that the packing contact between Phe53 and Ile50′ is lost (*i.e.* Fig. 6*a*). Once the inter-flap contacts are broken the flaps become much more mobile, while the β-hairpin becomes less structured. The end-point conformation entails hydrophobic interactions only within monomers (*i.e.* Fig. 6*b*). Hence, the crystal structures of apo HIV PR represent snapshots of this flap-opening mechanism. The apo 6× HIV PR and F53L mutant (2g69; Liu *et al.*, 2006) structures, with expanded but still 'curled' conformations, are intermediates between the 'curled' and fully 'open' states. The substrate-binding mechanism can be visualized with respect to the superposition in Fig. 3, in which the flaps translate away from the local twofold and hinge outward, breaking the 'top-to-top' packing contacts of the 'curled' conformation. Subsequently, upon substrate (*i.e.* TL-3) binding, the opposite faces of the flaps are brought into contact with each other.

Although conformational mobility of the flap domains of HIV PR has been recognized for some time, it is interesting that the unliganded enzyme appears to favor just two alternate flap conformations. Both are observed for the wild type, but to date drug-resistant mutants are only observed in either the 'curled' or 'open' states. As all currently approved antiviral drugs directed against HIV PR bind within the active site in the closed conformation, it may be advantageous to target the unliganded 'curled' and 'open' conformations in seeking novel binding sites for drug development. Small molecules binding to these states of HIV PR would inhibit the enzyme by preventing flap closure. This type of inhibitor may be more effective against the evolution of resistance, if it is less likely for mutants to arise that must not only reduce binding affinity but also do so without loss of requisite conformational mobility.

CDS, BET and JHE were supported by NIH grant GM48870. Additional support for BET and JHE came from NIH grant AI40882. We thank the staff of the Stanford Synchrotron Radiation Laboratory (SSRL) for expert technical support and access to resources. SSRL is a national user facility operated by Stanford University on behalf of the US Department of Energy, Office of Basic Energy Sciences. The SSRL Structural Molecular Biology Program is supported by the Department of Energy, Office of Biological and Environmental Research and by the National Institutes of Health, National Center for Research Resources, Biomedical Technology Program and the National Institute of General Medical Sciences. All figures were generated using *MoViT* v.1.2.1 (Pfizer, La Jolla, CA, USA).

References

Beck, Z. Q., Morris, G. M. & Elder, J. H. (2002). *Curr. Drug Targets Infect. Disord.* **2**, 37–50.
Berman, H. M., Westbrook, J., Feng, Z., Gilliland, G., Bhat, T. N., Weissig, H., Shindyalov, I. N. & Bourne, P. E. (2000). *Nucleic Acids Res.* **28**, 235–242.
Boden, D. & Markowitz, M. (1998). *Antimicrob. Agents Chemother.* **42**, 2775–2783.
Brünger, A. T. (1992). *Nature (London)*, **355**, 472–474.
Brünger, A. T., Adams, P. D., Clore, G. M., DeLano, W. L., Gros, P., Grosse-Kunstleve, R. W., Jiang, J.-S., Kuszewski, J., Nilges, M., Pannu, N. S., Read, R. J., Rice, L. M., Simonson, T. & Warren, G. L. (1998). *Acta Cryst.* D**54**, 905–921.
Buhler, B., Lin, Y. C., Morris, G., Olson, A. J., Wong, C.-H., Richman, D. D., Elder, J. H. & Torbett, B. E. (2001). *J. Virol.* **75**, 9502–9508.
Elder, J. H., Schnolzer, M., Hasselkus-Light, C. S., Henson, M., Lerner, D. A., Phillips, T. R., Wagaman, P. C. & Kent, S. B. (1993). *J. Virol.* **67**, 1869–1876.
Emsley, P. & Cowtan, K. (2004). *Acta Cryst.* D**60**, 2126–2132.
Heaslet, H., Kutilek, V., Morris, G. M., Lin, Y.-C., Elder, J. H., Torbett, B. E. & Stout, C. D. (2006). *J. Mol. Biol.* **356**, 967–981.
Hou, T. & Yu, R. (2007). *J. Med. Chem.* **50**, 1177–1188.
Jones, T. A., Zou, J.-Y., Cowan, S. W. & Kjeldgaard, M. (1991). *Acta Cryst.* A**47**, 110–119.
Kantor, R., Machekano, R., Gonzales, M. J., Dupnik, K., Schapiro J. M. & Shafer, R. W. (2001). *Nucleic Acids Res.* **29**, 296–299.
Kozal, M. (2004). *AIDS Patient Care STDS*, **18**, 199–208.
Kurt, N., Scott, W. R. P., Schiffer, C. A. & Haliloglu, T. (2003). *Proteins*, **51**, 409–422.
Kutilek, V. D., Sheeter, D. A., Elder, J. H. & Torbett, B. E. (2003). *Curr. Drug Targets Infect. Disord.* **3**, 295–309.
Lapatto, R., Blundell, T., Hemmings, A., Overington, J., Wilderspin, A., Wood, S., Merson, J. R., Whittle, P. J., Danley, D. E. & Geoghegan, K. F. (1989). *Nature (London)*, **342**, 299–302.
Lee, T., Laco, G. S., Torbett, B. E., Fox, H. S., Lerner, D. L., Elder, J. H. & Wong, C-H. (1998). *Proc. Natl Acad. Sci. USA*, **95**, 939–944.
Lee, T., Le, V.-D., Lim, D., Lin, Y. C., Morris, G. M., Wong, A. L., Olson, A. J., Elder, J. H. & Wong, C-H. (1999). *J. Am. Chem. Soc.* **121**, 1145–1155.
Leslie, A. G. W. (1992). *Jnt CCP4/ESF–EACBM Newsl. Protein Crystallogr.* **26**.
Lin, Y.-C., Brik, A., de Parseval, A., Tam, K., Torbett, B. E., Wong, C. H. & Elder, J. H. (2006). *J. Virol.* **80**, 7832–7843.
Liu, F., Kovalevsky, A. Y., Louis, J. M., Boross, P. I., Wang, Y.-F., Harrison, R. F. & Weber, I. T. (2006). *J. Mol. Biol.* **358**, 1191–1199.
Logsdon, B. C., Vickrey, J. F., Martin, P., Proteasa, G., Koepke, J. I., Terlecky, S. R., Wawrzak, Z., Winters, M. A., Merigan, T. C. & Kovari, L. C. (2004). *J. Virol.* **78**, 3123–2132.
Martin, P., Vickrey, J. F., Proteasa, G., Jimenez, Y. L., Wawrzak, Z., Winters, M. A., Merigan, T. C. & Kovari, L. C. (2005). *Structure*, **13**, 1887–1895.
Murshudov, G. N., Vagin, A. A. & Dodson, E. J. (1997). *Acta Cryst.* D**53**, 240–255.
Navia, M. A., Fitzgerald, P. M., McKeever, B. M., Leu, C. T., Heimbach, J. C., Herber, W. K., Sigal, I. S., Darke, P. L. & Springer, J. P. (1989). *Nature (London)*, **337**, 615–620.
Painter, J. & Merritt, E. A. (2006*a*). *Acta Cryst.* D**62**, 439–450.
Painter, J. & Merritt, E. A. (2006*b*). *J. Appl. Cryst.* **39**, 109–111.
Pettit, S. C., Sheng, N., Tritch, R., Erickson-Viitanen, S. & Swanstrom, R. (1998). *Adv. Exp. Med. Biol.* **436**, 15–25.
Pflugrath, J. W. (1999). *Acta Cryst.* D**55**, 1718–1725.
Prabu-Jeyabalan, M., Nalivaika, E. A., King, N. M. & Schiffer, C. A. (2003). *J. Virol.* **77**, 1306–1315.
Prabu-Jeyabalan, M., Nalivaika, E. A., Romano, K. & Schiffer, C. A. (2006). *J. Virol.* **80**, 3607–3616.
Prabu-Jeyabalan, M., Nalivaika, E. & Schiffer, C. A. (2002). *Structure*, **10**, 369–381.

Read, R. J. (1986). *Acta Cryst.* A**42**, 140–149.
Reiling, K. K., Endres, N. F., Dauber, D. S., Craik, C. S. & Stroud, R. M. (2002). *Biochemistry*, **41**, 4582–4594.
Rose, R. B., Rose, J. R., Salto, R., Craik, C. S. & Stroud, R. M. (1993). *Biochemistry*, **32**, 12498–12507.
Scott, W. R. & Schiffer, C. A. (2000). *Structure*, **8**, 1259–1265.
Shao, W., Everitt, L., Manchester, M., Loeb, D. D., Hutchinson, C. A. & Swanstrom, R. (1997). *Proc. Natl Acad. Sci. USA*, **94**, 2243–2248.
Spinelli, S., Liu, Q. Z., Alzari, P. M., Hirel, P. H. & Poljak, R. J. (1991). *Biochimie*, **73**, 1391–1396.
Studier, W. F., Rosenberg, A. H., Dunn, J. J. & Dubendorff, J. W. (1990). *Methods Enzymol.* **185**, 60–89.
Swanstrom, R. & Erona, J. (2000). *Pharmacol. Ther.* **86**, 145–70.
Swanstrom, R. & Wills, J. (1997). *Retroviruses*, edited by J. Coffin & S. Hughes, pp. 263–334. New York: Cold Spring Harbor Laboratory Press.
Tóth, G. & Borics, A. (2006). *J. Mol. Graph. Model.* **24**, 465–474.
Tozser, J., Yin, F. H., Cheng, Y.-S. E., Bagossi, P., Weber, I. T., Harrison, R. W. & Oroszlan, S. (1997). *Eur. J. Biochem.* **244**, 235–241.
Vagin, A. A. & Teplyakov, A. (2000). *Acta Cryst.* D**56**, 1622–1624.
Wlodawer, A., Miller, M., Jaskolski, M., Sathyanarayana, B. K., Baldwin, E., Weber, I. T., Selk, L. M., Clawson, L., Schneider, J. & Kent, S. B. (1989). *Science*, **245**, 616–621.